Investigation of the small-scale statistics of turbulence in the Modane S1MA wind tunnel

Mickaël Bourgoin, Christophe Baudet, Swapnil Kharche, Nicolas Mordant, Tristan Vandenberghe, Sholpan Sumbekova, Nickolas Stelzenmuller, Alberto Aliseda, Mathieu Gibert, Philippe-E. Roche, et al.

Noname manuscript No.
(will be inserted by the editor)

Investigation of the small scale statistics of turbulence in the Modane S1MA wind-tunnel

M. Bourgoin[1,4] · **C. Baudet**[1] · **S. Kharche**[1] · **N. Mordant**[1] · **T. Vandenberghe**[1] · **S. Sumbekova**[1] · **N. Stelzenmuller**[1] · , **A. Aliseda**[1,2] · **M. Gibert**[3] · **P.-E. Roche**[3] · **R. Volk**[4] · **T. Barois**[4] · **M. Lopez Caballero**[4] · **L.Chevillard**[4] · **J.-F. Pinton** [4] · **L. Fiabane**[5] · **J. Delville**[6,+] · **C. Fourment**[6,+] · **A. Bouha**[7] · **L. Danaila**[7] · **E. Bodenschatz**[8] · **G. Bewley**[8] · **M. Sinhuber**[8] · **A. Segalini**[9] · **R. Örlü**[9] · **I. Torrano**[1,10] · **J. Mantik**[11] · **D. Guariglia**[12] · **V.Uruba**[13] · **V. Skala**[13] · **J. Puczylowski**[14] · **J.Peinke**[14]

Received: date / Accepted: date

Abstract This article describes the planning, set-up, turbulence characterization and analysis of measurements of a passive grid turbulence experiment that was carried out in the S1MA wind-tunnel from ONERA in Modane, in the context of the ESWIRP European project. This experiment aims at a detailed investigation of the statistical properties of turbulent flows at large Reynolds numbers. The primary goal is to take advantage of the unequaled large scale dimensions of the ONERA S1MA wind tunnel facility, to make available to the broad turbulence community high quality experimental turbulence data with unprecendented resolution (both spatial and temporal) and accuracy (in terms of statistical convergence). With this goal, we designed the

1. Univ. Grenoble Alpes, CNRS, Grenoble INP*, LEGI, F-38000 Grenoble, France. · 2. Department of Mechanical Engineering, University of Washington, Seattle, Washington 98195-2600, USA. · 3. Institut Néel, CNRS, F-38000 Grenoble, France. · 4. Univ. Lyon, Ens de Lyon, Univ. Claude Bernard, CNRS, Laboratoire de Physique, F-69342 Lyon, France. · 5. IRSTEA, Rennes, France. · 6. Institut PPrime, CNRS/Universit de Poitiers, France. · 7. CORIA, CNRS/Universit de Rouen, France. · 8. MPIDS for Dynamics and Self Organization, Göttingen, Germany. · 9. KTH, Stockholm, Sweden. · 10. University of Mondragon, Spain. · 11. ETW, Kohln, Germany. · 12. Von Karman Institute, Sint-Genesius-Rode, Belgium. · 13. Academy of Science of the Czech Rep., Prague, Czech Rep. · 14. University of Oldenburg, Germany.
+ Carine Fourment and Joel Delville died in a terrible car accident on their way back from Modane, where the experiment presented in this document was carried out. We miss them immensely.

largest grid generated turbulence experiment planned and performed to date. Grid turbulence is a canonical flow known to produce almost perfectly homogeneous and isotropic turbulence (HIT) which remains a unique framework to investigate fundamental physics of turbulent flows. Here, we present a brief description of the measurements, in particular those based on hot-wire diagnosis. By comparing results from classical hot-wires and from a nano-fabricated wire (developed at Princeton University), we show that our goal of resolving down to the smallest dissipative scales of the flow has been achieved. We also present the full characterization of the turbulence here, in terms of turbulent energy dissipation rate, injection and dissipation scales (both spatial and temporal) and Reynolds number.

Keywords Turbulence

1 Introduction

The first scientific observation of turbulence probably dates back to Leonardo Da Vinci [11], who named, for the first time in history, *turbulenza* the complex swirling motion of water. Leonardo's drawings already emphasize two of the main properties of turbulence: its randomness and its multi-scale aspects, with small random eddies being embedded in larger ones. Since then, although our understanding of the phenomenon has significantly progressed, no complete framework has yet emerged which is able to fully explain the origin and the dynamics of turbulence. The pioneering work by Reynolds showed that turbulence appears whenever the viscous forces are small compared to the driving inertial forces. In practice, this includes most macroscopic natural and technological flows, which makes turbulence an enormously important open question, and a challenge for future research. Beyond its fundamental interest, piercing the mysteries of turbulence may help improving aerodynamics design, weather forecasting, understanding the evolution of stars, blood flow modeling, and a myriad of other applications.

Paradoxically, although turbulence can be described from well-known first principles in continuum mechanics, namely using the Navier-Stokes equations, it remains an unsolved problem in classical physics. This has to be related back to the enormous number of degrees of freedom involved in the problem, which is itself related to the intrinsic properties of the Navier-Stokes equations: non-locality and non-linearity. This degree-of-freedom complexity increases as a power law of the Reynolds number $Re = UL/\nu$ in the flow [6,9], with U being the typical velocity of the flow, L its typical large scale and ν the viscosity of the fluid. As a consequence, a simple local description of the flow fails to give a clear view of the underlying mechanisms governing the overall multi-scale motion of turbulence. An alternative strategy, starting with the Reynolds decomposition, another piece of seminal research, is to adopt a statistical description of turbulence, based on the experimental observation that a flow stirred at large scale develops fluctuations at small scales, which are

statistically stationary. This picture was later confirmed by numerous massive numerical simulations: when forced at large scales (even deterministically [13]) the Navier-Stokes equations develop statistically homogeneous and stationary fluctuations. This observation serves as a cornerstone of modern studies in turbulence, aiming to provide an accurate statistical description of turbulence.

Richardson played an important role in building such a statistical approach, proposing in the 1920s, a multi-scale description of the phenomenon in terms of an energy cascade, where turbulence appears as a hierarchy of random eddies with sizes ranging from the scale where energy is injected (which could be thousands of meters for atmospheric flows, as an example) down to the scale where it is dissipated by viscosity (which could be in the microns). This range of scales (between injection and dissipation) bounds the inertial range of turbulence. This qualitative description was put in a more quantitative framework by numerous scientists, including Heisenberg, Weizsäcker, Onsager and A. Kolmogorov in 1941 [7] who developed a phenomenological description of the turbulent cascade, based on dimensional considerations and assuming homogeneous and isotropic turbulence (HIT) with a self-similarity hypothesis of statistical properties of eddies within the inertial range of scales. In the Kolmogorov 1941 phenomenology (referred to as K41), the statistical properties of turbulence are mostly characterized by one single parameter: ϵ, the average energy dissipation rate (which in stationary conditions equals the average energy injection rate). One of the big successes of K41 is the prediction of the spectrum of the kinetic energy of turbulent eddies (the celebrated $k^{-5/3}$ law). However, as rapidly objected by Landau, K41 fails to predict one important statistical property of turbulence known as intermittency. This is physically represented by the fact that energy dissipation (which is related to the viscous friction between fluid elements at small scales) is highly unevenly distributed in space. To account for intermittency, Kolmogorov proposed in 1962 [8] a refined version of his self-similar phenomenology, including Obukhov suggestion that the energy dissipation rate exhibits strongly non-Gaussian fluctuations. However, the description of intermittency and its origins are still unknown, and its modeling remains an active field of research [6, 2] whose development still requires more accurate experimental evidence, as some of the most measurements used as references for intermittency date back to the 90's [1]).

To finish this brief description of the state of the art of turbulence, we should also mention one of the most important applications of turbulence which is its ability to mix rapidly and efficiently. The mixing problem is usually referred to as the passive scalar problem. It corresponds to the investigation of the diffusion of a scalar (for instance the concentration field of a dye, or a temperature field) which does not affect the main carrier flow. The statistical characterization of the passive scalar field in turbulent conditions also reveals a strong small scale intermittency, with important and uneven fluctuations of the scalar dissipation. The origins of this intermittency and its connection to intermittency (either Eulerian or Lagrangian) of the carrier flow remain open questions. Concerning the scalar, other important questions remain open, such

the rate at which the mixing process is accelerated by the turbulence and the influence of the Reynolds number of the carrier flow on this process.

In this context, there is a strong need for high quality data in the scientific and engineering communities, suited to test, validate and calibrate models and simulations of turbulent flows (for the Eulerian approach, the Lagrangian description and the passive scalar problem). The demand is particularly important concerning homogeneous and isotropic turbulence (which remains the preferred field to investigate fundamental properties of turbulence) at large Reynolds number (for which asymptotic limits are generally investigated to derive scaling laws of turbulent dynamics). State of the art strategies to produce high Reynolds numbers in laboratory experiments consist of injecting a huge amount of mechanical energy in a small volume of fluid. One of the most studied configurations of this type is obtained by considering the flow between two counter-rotating impellers in a cylindrical vessel full of water (the so-called von Karman flow). Such swirling flows have been extensively investigated in the turbulence community [7,10,11]. However this geometry has several drawbacks. The main one is the strong anisotropy of the flow which makes any comparison to models and simulations complicated and ambiguous. The second is that the small scales at which effects such as intermittency become important are extremely small (of the order of microns for spatial scales and milliseconds for temporal scales), testing the limits of the resolution of classical instrumentation. Another recent strategy to achieve high Reynolds number turbulence rely on cryogenic flows using liquid or gaseous Helium which has a very low viscosity. However, fluid dynamics measurements in such cryogenic conditions are still in their infancy. The best state of the art configuration to produce HIT remains grid-generated turbulence in wind-tunnels [12]. This turbulence is produced by the interaction of the wake from the rods forming a grid with appropriate geometry. However the limited dimensions of academic wind-tunnels only allow moderate Reynolds numbers to be reached, limiting the possibility to explore in detail the Reynolds number effects on inertial scalings and intermittency.

The goal of our project is to contribute to the effort in untangling the statistical description of turbulence by offering the scientific community a unique database of fully-resolved experimental data of turbulent flow in homogeneous and isotropic conditions at large Reynolds number. In an intermediate timeframe, this database is intended to become “open source” and to be made available to the scientific community. It will be a precious tool at several levels : (i) as a reference and a standard of turbulence properties for validation and calibration of other experiments and numerical simulations(DNS, LES, RANS, etc.) ; (ii) for the fundamental understanding of turbulence physics and (iii) for the development, tuning and calibration of accurate models. Building such a database requires the ability to measure accurately scale by scale statistical properties of turbulence, with high spatial and temporal resolution over the entire range of relevant scales, including inertial scales and dissipative scales.

These considerations motivated our project to produce and investigate grid-generated turbulence in the S1MA windtunnel in Modane. The unique size of this facility (typically one order of magnitude larger than usual academic windtunnels) enabled the production of high Reynolds number turbulence with fully resolvable dissipative scales and fulfilling the double condition $\eta \ll L \ll D$: (i) a dissipation scale η much smaller than the energy injection scale L, as requires to develop real inertial range scalings and (ii) an injection scale L much smaller than the size of the facility D in order to avoid undesired confinement effects from the walls. A large scale grid (10 m in diameter, with a mesh size of 0.625m) was used as a turbulence generator, as it is known to produce canonical homogeneous and isotropic turbulence. Building and installing such a large grid was one of the major challenges of this project. This required not only to design a unique grid using inflatable structure technology, but also to adapt the S1MA wind tunnel in order to install the grid in it.

Additionally, in order to build a database as complete as possible, many different complementary measurements were implemented during the experiment, giving access to Eulerian and Lagrangian description of turbulence statistics:

1. Hot-wire anemometry
2. Laser cantilever anemometry (LCA)
3. miniature-Pitot tubes
4. Lagrangian Particle Tracking Velocimetry (PTV)
5. Vortical acoustic scattering

Due to technical issues, Lagrangian PTV measurements were unsuccessful during the campaign and Vortical acoustic scattering measurements have not been analyzed yet. LCA and miniature-Pitot tubes measurement have been partially processed while hot-wire anemometry measurements has now been fully assessed. The present article aims primarily at presenting the experiment, the properties of the investigated turbulence (injection and dissipation scales, isotropy, Reynolds number, etc.) and the quality of the acquired data (in particular in terms of the small scale spatial resolution of the measurements) hoping that this database will serve as a reference in the future for the turbulence research community. This document is organized as follows: section 2 details the main preparation stages of the experiment, section 3 describes some of the measurements which have been performed and section 4 gives a detailed characterization of the turbulence generated, based on hot-wire anemometry measurements.

The experiment took place from July 7th to 11th 2014, in the S1MA wind tunnel of ONERA in Modane (France) as part of the ESWIRP initiative. Our experimental campaign was sadly affected by a tragic event. On the day after the campaign ended, two of our colleagues (Carine Fourment and Joel Delville) from the PPrime Laboratory (University of Poitiers, France) died in a terrible car accident on their way back from Modane. Carinne and Joel

had designed and operated the most beautiful instrument of the campaign: a multi-probe array of almost 23 hot-wires with the capability to characterize the full spatio-temporal multi-scale dynamics of turbulence. This sad event was a terrible scientific and human loss for the team and for the community. The data acquired during the campaign is still been processed. The present manuscript, therefore, focuses on describing the experimental implementation and on the characterization of the turbulence, exploiting primarily hot-wire anemometry data and analysis.

2 The experiment

Preparing this experiment required several challenging tasks to be solved. First, a grid turbulence experiment of the scale conducted here had never been performed before and no precedent existed on how to manufacture such a large scale grid. Second, introducing such a grid in S1MA induced a much higher pressure drop than usual models tested in this wind tunnel. This constraint needed to be taken into account in the design of the experiment. Third, as previously highlighted, many simultaneous experimental rigs had to be accommodated, requiring a dedicated instrumentation platform. The following sections briefly discuss the main aspects of the experiment planning and setup.

2.1 The wind tunnel

The ONERA S1MA wind tunnel (located in the town of Modane in the French Alps) is the largest sonic wind tunnel in the world. Figure 1 shows a schematic of the facility where its unique dimensions can be appreciated. The test section is 8m in diameter and 14m long. The flow is generated by two counter-rotating fans (15m in diameter), each of which is directly driven by a Pelton turbine moved by a water fall with a total hydraulic power up to 88 MW, allowing it to achieve Mach numbers of order 1 in normal operating conditions. The present study concerns, however, a quite unusual operating point for the tunnel, as a turbulence-generating grid with a blockage section of 35% was inserted in the convergent section of the tunnel, about 8m upstream of the entrance of the test section (see next section). This resulted in a significant increase of the pressure drop across the tunnel compared to usual operating conditions where the blockage section of models in the test section rarely exceeds 1%. As a consequence, in order to keep the total pressure drop of the order of the maximum admissible pressure drop typically sustained by the fans (of the order of 250Pa), the maximum velocity at which the tunnel was operated in this experiment did not exceed 45m/s in the test section. At this velocity, the required mechanical power to drive the fans was of the order of 3MW, hence much less than the maximum available power, but the pressure drop in the presence of the grid was comparable of the maximum admissible pressure drop.

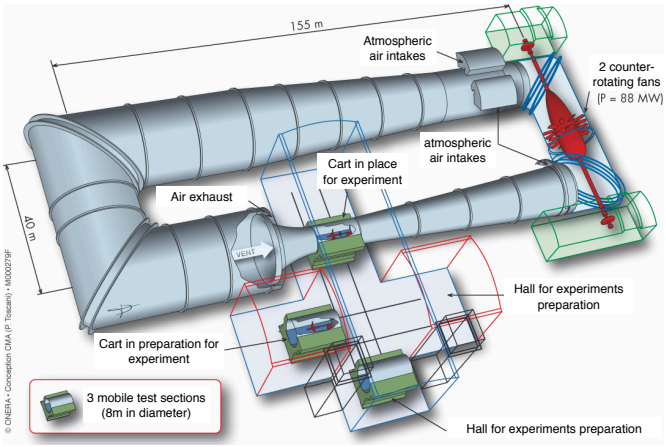

Fig. 1 Onera S1MA wind tunnel.

2.2 The grid

Initially, the turbulence-generating grid was proposed to be a metallic structure of about 8m in diameter, mounted at the entrance of the test section in S1MA. Empirical laws for turbulence generation [5] suggest an optimal solidity of the grid between 30% and 40%. As discussed in the previous section, it became rapidly evident that such a blockage ratio would impose a pressure drop that went far beyond the capabilities of the wind-tunnel. Reasonable pressure drops (not exceeding 250Pa) would require to lower the solidity of the grid to around 20%, at which point the turbulence generation becomes very inefficient. The solution found was to place the grid not at the entrance of the test section, but in the convergent section of the tunnel, upstream of the test section, where the local diameter is 10m (up from 8 m in the test section), so that the pressure drop for a given solidity is reduced by about 35%. The problem, then, moved from an aerodynamic issue to a structural issue, as building a heavy metallic grid (the estimated weight for an aluminum structure was of the order of 2 tons) in the convergent section of S1MA was not allowed. We explored, therefore, the possibility to build a light inflatable structure. The study of the feasibility of this solution was contracted to CERTEC®, a french company specialized in inflatable structures at all scales, in close collaboration with LEGI (the scientific partner and ONERA in this experimental campaign). The final design consisted in an inflatable grid, with a solidity of 33%, made of cylindrical Polyvinyl chloride tubes, inflated with air pressurized to 1-5 bar, with a diameter of 120mm and a mesh spacing of 625mm. The horizontal cylinders were all coplanar, and all the vertical cylinders also occupying another, contiguous, plane. The pictures in figure 2 show the first test of assembly of the grid, in September 2013 and the grid in its final position in the convergent section of S1MA.

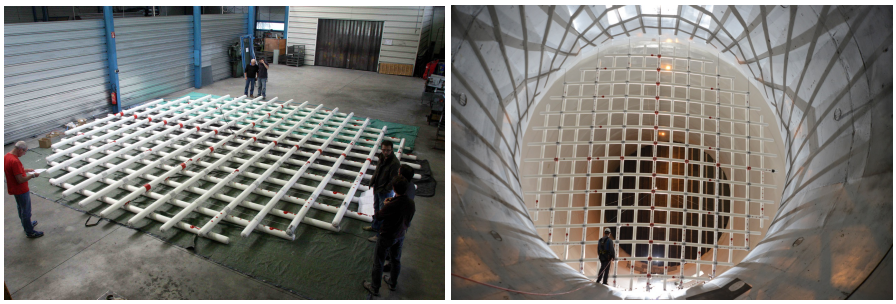

(a) (b)

Fig. 2 (a)First assembly of the grid. (b) Final assembly of the grid in the convergent section of S1MA windtunnel.

2.3 The instrumentation platform

A dedicated instrumentation platform capable of hosting all the planned sensors and apparatuses for the diagnosis of the turbulence was specially designed for the campaign. Many sensors and probes required to have their corresponding instruments (amplifiers, anemometers, conditioners, etc.) as close as possible, in order to limit cable length and hence improve signal-to-noise ratio, response time, resolution, etc.. This required to design an instrumentation trunk underneath the platform, with an aerodynamic profile, to limit the additional pressure drop induced by the platform in the test section. The picture in figure 3 shows the instrumentation platform during the test, with most of the sensors mounted. The different instruments and corresponding measurement techniques are discussed in section 3.

2.4 Adapting S1MA for the project

The unusual configuration of the experiment, compared to usual model tests in S1MA required several modifications to be performed:

1. Installing the grid in the convergent section required 7 vertical cables to be set inside the convergent section, to fix the grid and hold 7 500kg-weights underneath in order to keep the cables under tension and limit the deformation of the grid. This was the most complex modification required in S1MA.
2. Mounting of the platform in the test section (which needed to be able to translate along the streamwise direction, in order to allow the scanning of turbulence properties at different positions downstream the grid) required to install dedicated rails along the floor of the test section.
3. Particle tracking experiments required to mount particle generators upstream of the measurement volume. This was done thanks to two vertical cables mounted across the test section, where droplet injectors and bubble generators were attached.

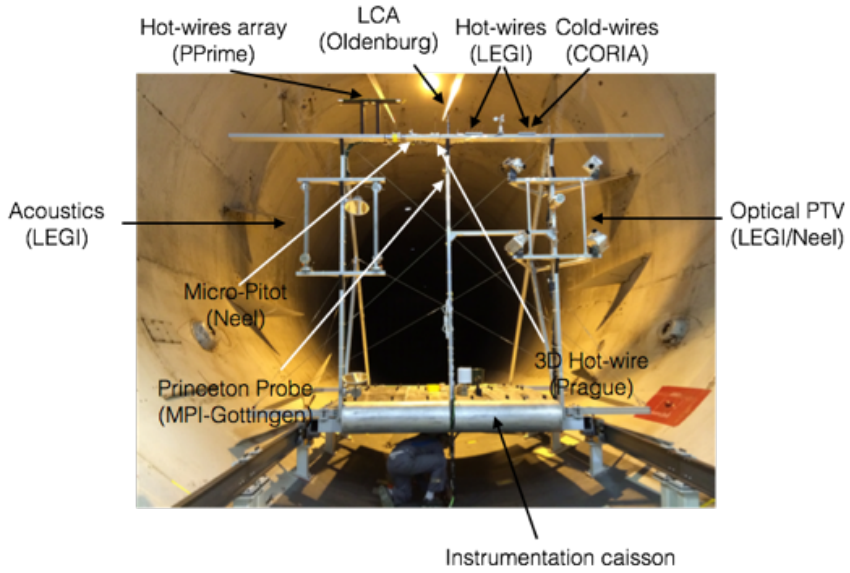

Fig. 3 Instrumentation platform

3 The measurements

3.1 Global view of the measurement campaign

The main goal of the experiment was the characterization of the smallest scales of homogeneous isotropic turbulence. Hence, most of the measurements were carried out with the instrumentation platform at the farthest position downstream of the grid (corresponding to nearly 40 grid mesh lengths), where the turbulence is fully developed, with optimal homogeneity and isotropy properties. Wind velocity was varied between 20 and 45m/s. For optimal statistical convergence, measurements as long as 2 hours of continuous acquistion were carried out at a given wind speed. To understand the need for such long running time, recall that the typical correlation scale of the flow studied is given by the mesh size (a fraction of it in the present case due to the contraction effect). If we take 15 cm as the right order of magnitude, a run of 2 hours at the velocity of 30 m/s warrants that $30 \times 7200/0.15 = 1.4 \cdot 10^6$ correlation scales of the flow are effectively sampled, which ensures excellent statistical convergence. Shorter acquisition time runs were also performed at other positions, in order to briefly characterize the turbulence decay downstream of the grid by monitoring simple statistical indicators such as the mean turbulent kinetic energy per unit mass, which is directly given by the variance of the velocity fluctuations.

The following sections give more details of the different complementary measurements performed for the characterization of the turbulence. We also present the first results on classical turbulence statistics. We stress that the

experiment was carried out in July 2014 and that tens of Tera-bytes of data were collected. The building, processing and quality assessment of this immense database represents a significant effort, which is now almost complete regarding the hot-wire anemometry measurements. We also note that the goal of the present article is to present the existing database and to give the classical indicators of the turbulence explored, in particular in terms of Reynolds number, turbulent energy dissipation rate, injection and dissipation scales (both temporal and spatial). We do not aim here to address any particular scientific question of turbulence research.

In this section, devoted to present and assess the quality of the different measurements achieved during the campaign, we briefly describe some of the other probes used during the experiment (including Laser Cantilever Anemometer (LCA) and miniature-Pitot tube), although the corresponding data is not yet fully calibrated and validated and will therefore not be presented in detail. The next section is therefore devoted almost entirely to present the characteristics of the investigated turbulence from hot-wire anemometry measurements.

3.2 Hot-wire anemometry

Methodology. Hot wire anemometry remains the most typical high resolution measurement for the accurate characterization of the velocity fluctuations in wind tunnel turbulent flows. The principle is very simple: a small conducting wire (typically a few microns in diameter and less than a millimeter in length) is heated above the ambient temperature; the convective heat transfer induced by the surrounding flow then tends to cool the wire and, hence, to modify its electrical conductivity, which is monitored and whose fluctuations are related to the velocity after a proper calibration has been done. The most common measurement protocol is CTA (Constant Temperature Anemometry): the wire is inserted in a Wheastone bridge, which is kept balanced with a feedback loop where the electrical current is dynamically adjusted so that the Joule dissipation in the wire dynamically varies to maintain the wire at constant resistivity (and hence at constant temperature). As a consequence the voltage feeding the bridge fluctuates, reflecting the velocity fluctuations of the velocity around the wire. The relation between voltage fluctuations and velocity can be calibrated according to King's law. Each wire needs to be individually calibrated, and the calibration parameters depend on the ambient temperature which means that, either, an accurate temperature-dependent calibration in needed, or one has to recalibrate the sensors for each given experimental condition. This motivated conducting several ramps in velocity during the measurement campaign: these ramps were necessary to test the calibration of the hot-wires and to recalibrate them if necessary. The spatial and temporal resolution of the hot wire measurement is directly related to the dimensions of the wire. The smaller the wire, the better the spatial resolution but also the better the frequency response, as smaller wires have less thermal inertia and hence respond faster to tur-

bulent fluctuations. Additionally, in order to have an appropriate directional measurement (responding specifically to one of the velocity components), the length to diameter ratio of the wire must be of the order of 100 or larger. For instance, a wire with a diameter of 5 microns must be at least 500 microns long. The effective spatial resolution is then limited by the length of the wire.

In the present experiment several types of hot-wires were used:

1. Six classical single-component wires from LEGI, with diameters between 1.25 and 5 microns and a sensitive length in the order of 400 microns. The signal from the 6 wires was simultaneously acquired using a Dantec Streamline Constant Temperature Anemometer (CTA) embedded in the measurement platform inside the test section, so that short cables (5 m long) could be used to connect the hot-wires to the anemometer).
2. One three-component cross wire from the Prague group, with diameters of 5 microns, measuring simultaneously the 3 components of the velocity. Each hot-wire was also connected to the Dantec Streamline CTA with a 5 m cable).
3. A nano-fabricated wire, designed at Princeton U. [3], known as NSTAP, with very high resolution was also tested by the Göttingen group (which has a separate partnership with the Princeton group developing this sensor). Dimensions of the sensitive part of the NSTAP hot-wire are 100nm x 300nm x 30 μm. The NSTAP hot-wire was monitored with an AA Labs CTA, located outside the tunnel, with a 20 m cable.
4. An array of 23 single wires with logarithmic spacing along a linear array, giving access to transverse correlations of velocity fluctuations, from the Poitiers group who had prepared a unique measurement device composed of 2.5 micron in diameter, 600 micron long single-component wires. Our colleagues from Poitiers were victims of a fatal car accident on their way back from Modane after the campaign. It is unlikely that their data will ever be retrieved.

In order to compare resolution issues of the hot-wire measurements, we briefly discuss here the spectra of different measurements, in particular comparing the data from classical hot-wires to the nano-fabricated NSTAP wire. Figure 4a shows the typical Eulerian power spectral densities measured with our 6 classical single hot-wires. It can be seen that all 6 hot-wires behave almost identically at large and inertial scales, with a well defined $f^{-5/3}$. Their small scale behaviour is not, however, equally resolved. Hot-wire #6 is clearly defective at small scales with a marked peak around 5 kHZ. The hot-wires have similar small-scale responses, with a decay in the spectrum around 2 kHz which, as it will be emphasized later, correctly captures the small dissipative scales of the flow. (Note that for the present discussion on spectral resolution, we have kept the temporal spectra of the original hot-wire signals, but a Taylor hypothesis will be applied later on to define the spatial Eulerian spectra). It should be noted, however, that parasite peaks on the spectrum are more or less pronounced depending on the wire and the smallest resolved scales (at high frequency) before the emergence of high frequency noise varies slightly

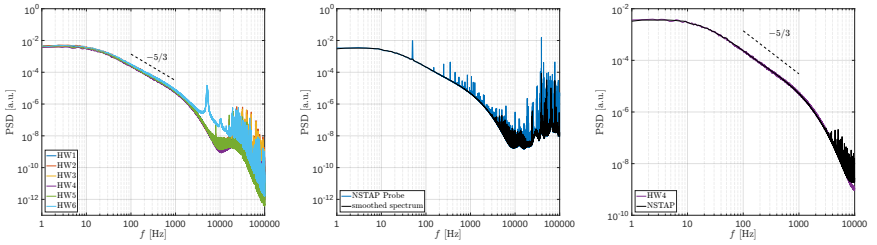

(a) (b) (c)

Fig. 4 Spectra of velocity fluctuations measured for different wind velocities with the traditional hot-wires (a) and spectrum measured at 25m/s with the 6 classical single hot-wires. (b) Corresponding spectrum measures with the nano-frabricated NSTPA probe (blue). The black line simply represented the spectrum smoothed with a median filter in order to eliminate the narrow parasite peaks, most of which correspond to harmonics of 50 Hz (the frequency of AC electricity supplies). (c) Superposition of the spectrum from HW4 in figure (a) and of the smoothed NSTAP spectrum in figure (b). The almost perfect superposition, in particular at the highest frequencies, supports the fact that the cut-off (around 2kHz) after the inertial $f^{-5/3}$ regime corresponds to the physical dissipative range of the probed turbulence.

from wire to wire, marginally affecting the effective dynamical range of each probe. Of all the measurements showed, hot-wire #4 presents the best spectral response, with a dynamical range spanning 6 orders of magnitude (between 10^{-2} at low frequency down to 10^{-8} at high frequency, before noise emerges at frequencies above 10 kHz. It is important to note that the discussed differences in the quality of the recorded signals are small (except for hot-wire #6) and can be due to tiny differences in the quality of the welding of the hot-wires on the probe, to tiny imperfections of the connectors, etc. Such an analysis of the spectral response of the hot-wires has been systematically carried out for each recording during the campaign, allowing to select the one with the best response fro each condition among the different hot-wires.

Figure 4b shows the corresponding spectrum measured now with the nano-fabricated NSTAP hot-wire. First, we observe that the signal from the NSTAP presents some noisy peaks at 50 Hz and harmonics, which are not present in the classical hot-wire measurements. It is important to stress that this is not an intrinsinc defect of the NSTAP wire, but the result of the length (20 m) of the cable connecting the probe to the anemometer which unfortunately, due to practical reasons could not be located within the measurement caisson like for the other probed, but had to be located outside the tunnel. This resulted in a strong amplification of 50 Hz parasites (and harmonics). The black line in figure 4 shows the same spectrum simply smoothed with a narrow median filter.

In Figure 4c, we have superimposed the spectrum from hot-wire #4 in figure 4a and the smoothed spectrum from the NSTAP nano-fabricated hot-wire. Interestingly both spectra overlap almost perfectly. In particular, the cut-off after the $f^{-5/3}$ inertial range is identically captured by both probes. Considering the difference in size between both probes (recall that the length

of the classical hot-wires was of the order of 500 microns, while the NSTAP probe was only 30 microns), this shows that the cut-off is indeed associated to the physical dissipative scales of the turbulence studied and does not result from probe finite-size effects. Detailed estimations of all relevant scales of the turbulence are presented in section 3.4. The NSTAP probe, therefore, validates the capacity of the classical probes to actually resolve the smallest scales of the flow. Due to the lower level of noise in the signal from the classical probes, the characterization of the flow presented in section 3.4 was mostly performed using the classical wire signals. The quality assessment presented here also shows that, should we have the chance to repeat these measurements, it would be critical to use shorter cables to get the full benefit of the resolution of the NSTAP probes.

3.3 Laser Cantilever Anemometer (LCA)

The 2D-Laser Cantilever Anemometer has been developed at the University of Oldenburg [10] as an alternative to commercial x-hot-wires. It features a spatial resolution of about 160 μm and a temporal resolution of about 100kHz.

Measuring principle. The underlying principle utilized in the 2D-LCA is the detection of the deformation of an one-sided fixed microstructured cantilever that is exposed to a fluid flow. For a straight inflow, i.e. a flow direction perpendicular to the cantilever surface, the deformation is a response to the drag force F_{drag}, that is given by:

$$F_{drag} = C_d(u)\rho A u^2. \tag{1}$$

Here, u is the flow velocity, $C_d(u)$ is the drag coefficient, ρ is the density of the fluid and A is the area of the cantilever that is facing the flow. For an oblique flow, *i.e.* flow at an angle of attack $\alpha \neq 0$, the total deformation of the cantilever is observed to be a superposition of bending and twisting. In that case the quantities A and $C_d(u)$ become functions of α and equation above becomes:

$$F_{drag} = C_d(u, \alpha)\rho A(\alpha) u^2. \tag{2}$$

The detection of the deformation is accomplished by means of the laser lever arm principle that is also used in atomic force microscopy. For that purpose,

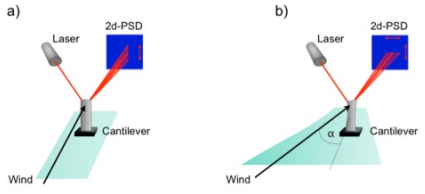

Fig. 5 Principle of the Laser Cantilever Anemometer: (a) 1D version, (b) 2D version.

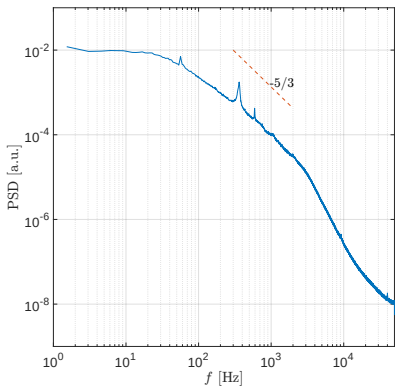

Fig. 6 Spectrum of velocity recorded with the LCA for a mean wind speed $U = 44$ m/s.

a laser provided by a laser diode ($\lambda_{laser} = 660$nm, Power = 5mW) is focussed onto the tip of the cantilever. The resulting reflection beam is tracked using a 2D-position sensitive device (2D-PSD) with an active area of 4mm×4mm. This principle is schematically illustrated in figure 5 for both deformation modes.

Figure 6 shows a typical spectrum of velocity measured with the LCA (obtained for the highest wind-speed, $U = 45$m/s). The spectrum shows a relatively well defined inertial range with a behavior close to $f^{-5/3}$ (although visibly less steep). The dissipative cut-off is observed to occur around 3kHz, in agreement with the hot wire measurements at similar wind-speed. Some spurious peaks are nevertheless present on the spectrum, which are likely related to parasite mechanical vibration due an defect of the holder used to mount the sensor on the measurement platform detected *a posteriori*. This unfortunate mechanical problem makes the present LCA data very likely not suited for a detailed multi-scale analysis of the turbulence, although it is still likely to be valuable to validate large scale statistical quantities (such rms velocity) and fine tune the calibration of hot-wires. Further quality assessment of the LCA data is in progress.

3.4 Miniature Pitot tubes

Two miniature Pitot tubes anemometers were specially designed and installed in alternance at Modane S1 wind-tunnel to measure the mean velocity and its more energetic fluctuations during the first 4 days of the experiment (7/7-10/7). Compared to hot wire anemometers, the key advantages of the miniature Pitot tubes are their robustness (in particular to particles impinging on the probe) and the fact that they do not need any calibration. Their main limitations are the spatial and temporal resolution, which is typically a few millimeters over a bandwidth up to few kHz. Given the typical velocity range in this very large scale experiment, the bandwidth limitation is the most strin-

gent one. The expected physical outcome from miniature Pitot tubes measurement includes the assessment of the flow turbulent intensity independently of the transducer and electronic sensitivities, and cross-check of the other sensors based on different velocity-measurement mechanisms (hot films and wires, cantilever, etc.). This diagnosis can be obtained from the Pitot tubes without any calibration (other than the geometric constant of the Pitot tube), and is extremely valuable to improve the quality of the more complex calibration for hot-wire probes. Another objective is to validate in a canonical grid-generated turbulent flow the specific sensor design, which has been originally designed to be deployed in cryogenic helium experiments, and was developed as part of the I^3 European project EuHIT.

Pitot tube #1. The nozzle (external diameter of 3 mm) and pressure reference taps of the Pitot tube #1 are following the NPL modified ellipsoidal-nosed standard (norm BS1042 and french norm AFNOR NFX10-112). Its Helmholtz resonance was around 4.2 kHz with a typical quality factor of 7. This Pitot tube evidenced very good immunity to acoustic and environmental electromagnetic noise. Indeed, the only detectable disturbances were the voltage-noise of the preamplifier (see below) and the Johnson-Nyquist thermodynamical noise from sensing resistors, both significantly below the velocity signal. Zeroing of the probe at null velocity was performed several times everyday to compensate for a slight drift. This Pitot tube #1 was used the first three days of the experiment.

Pitot tube #2. The Pitot tube #2 was operated only during the last day. Unfortunately, it picked up an energetic parasitic acoustic noise around 400 Hz, which prevented us from benefiting from its full dynamical range which was three times better than Pitot tube #1 (first intrinsic resonance at 13 kHz). The noise source may have been caused by the gas jet from the bubble seeding apparatus. Hence, the data processing focusses on the first Pitot tube.

Mounting, Electronics and data acquisition. Special attention was dedicated to the probe mountings both in term of stiffness, damping of vibrations from the support and flow invasiveness. The probe was located on the top horizontal bar of the probe rack, near the centre of it. The electronics powering circuitry consisted of the battery-driven DC voltage source and a temperature-compensation resistive bridge aimed at compensating the residual temperature dependence of the piezo-resistive Wheatstone bridge of the pressure transducer. On the measuring side, a preamplifier was inserted before a 16-bit ADC acquisition card with synchronous recording with two of the single-component hot-wires. Given the sharp cut-off of the Pitot tube signal above its first Helmholtz resonance, and the sampling frequency (> 200 kHz), no antialiasing filter was needed.

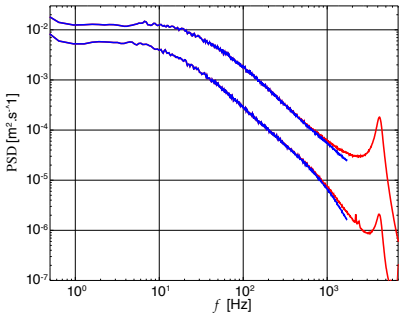

Fig. 7 Spectrum of velocity recorded with the miniature Pitot tube #1 for mean velocities 20 m/s and 45 m/s. The red curves represent the spectrum of the raw signal, where the Helmholtz resonance of the tube at 4.2 kHz can be seen. The blue lines simply show the same signal after removal of the Lorentzian peak.

Preliminary post-processing. As illustrated by the spectra shown in figure 7, the miniature Pitot tube is able to resolve a significant fraction of the inertial range. This ensures that an accurate estimation of the flow kinetic energy is possible from the velocity spectra (recall that the variance of velocity fluctuations σ_u^2 is given by the integral of the entire spectrum) since the most energetic part of the spectra is well-resolved in all conditions and the minor unresolved part of the spectrum at very high frequencies contribute only marginally to the integral. Hence, a precise assessment of the turbulence intensity (with upper and lower bounds) was performed using data from Pitot #1 and allowed cross-checking of hot-wire calibration. Deeper analysis and quality assessment of the miniature-Pitot tube data is in progress.

4 Turbulence properties

We present in this section the main characteristics of the turbulence studied: velocity PDFs, standard deviation, isotropy level, estimation of the turbulent energy dissipation rate ϵ, estimation of integral scales, estimation of dissipation scales and Reynolds number. These estimates are presented only for measurements carried out in the farthest position downstream from the grid (of the order of $X/M \approx 37$). Results presented in this section have been obtained from the classical hot-wire anemometry recording, selecting those hot-wires with the best quality assessment as discussed in the previous section. The estimation of the different statistical indicators is illustrated in the next sub-sections. Note that not all the signals and their corresponding estimations are shown. For clarity, we generally illustrate the estimation of the different indicators for only one mean wind velocity, and then we summarize in table 1 the results for the entire set of measurements.

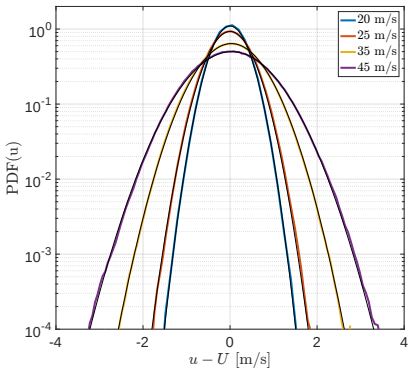

Fig. 8 Probability density functions of the velocity fluctuations measured at $X/M \approx 37$ for the 4 different mean wind speed investigated. Fluctuations are well described by a Gaussian distribution (represented by the black thin lines).

4.1 Velocity Probability Density Functions

Figure 8 represents the probability density functions (PDFs) of the streamwise velocity fluctuations measured at $X/M \approx 37$ for the four mean wind velocities explored in the experiment. As generally expected for grid-generated turbulence, we find that fluctuations are well described by a Gaussian distribution (shown by the thin black lines in figure 8). The corresponding standard deviation of the velocity fluctuations are $\sigma_u = 0.36$m/s - 0.42m/s - 0.59m/s - 0.79m/s when the mean wind velocities is $U = 20$m/s - 25m/s - 35m/s - 45m/s, showing a relatively constant turbulence intensity $\sigma_u/U \approx 1.7\%$, consistent with the independent assessment done with the miniature-Pitot tube. Additionally, measurements from the three-component hot-wire probe show that the anisotropy level, defined as the ratio between the streamwise and the spanwise velocity variances, is of the order of 20% at most, comparable to typical grid-generated turbulence laboratory experiments.

4.2 Estimation of large scales

We show in figure 9a the Eulerian autocorrelation function R_{uu} of the streamwise velocity measured for the highest mean wind speed investigated ($U = 45$m/s). R_{uu} is defined as

$$R_{uu}(\rho) = \frac{\langle u(x+\rho)u(x)\rangle}{\sigma_u^2}, \tag{3}$$

where $\langle\cdot\rangle$ stands for an ensemble average and where the spatial scale ρ is spanned here using a classical Taylor hypothesis (justified considered the low turbulence intensity of 1.7% of the velocity fluctuations) to convert a temporal increment τ along the recorded signal into a spatial increment $\rho = U\tau$, with U the mean wind velocity. The correlation function is found to be well-behaved

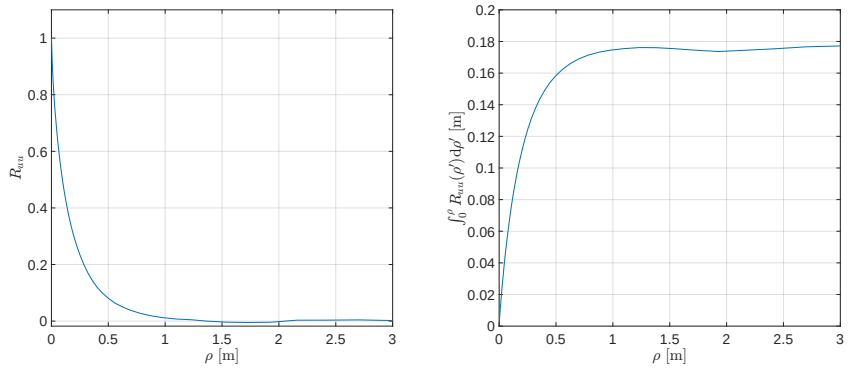

(a) (b)

Fig. 9 (a) Eulerian auto-correlation function R_{uu} of the streamwise velocity, measured at $X/m \approx 37$ for a mean wind speed $U = 45$m/s. (b) Cumulative integral of R_{uu}, whose asymptotic value gives the estimation of the integral scale L of the turbulence. Note that a well-behaved asymptotic plateau is indeed attained allowing for proper estimation of L.

and to decorrelate to zero at a typical scale of the order of 1m, consistently with the idea that the large scales in grid-generated turbulence are fixed by the mesh size of the grid. To be more quantitative, we can estimate the integral scale defined as

$$L = \int_0^\infty R_{uu}(\rho')\mathrm{d}\rho'. \tag{4}$$

Figure 9b shows the cumulative integral $\int_0^\rho R_{uu}(\rho')\mathrm{d}\rho'$. It exhibits a well defined asymptotic value at large spatial increments ρ, pointing to an integral scale of $L \approx 18$cm. The same procedure has been repeated for the other velocities tested, and the integral scale is found to marginally increase from $L \approx 15$cm to $L \approx 18$cm when the mean wind speed increases from 20m/s to 45m/s. Finally, we define the integral Eulerian time scale of the flow as $T_E = L/\sigma_u$. It is found to decrease from 0.42s down to 0.21s when the wind speed increases from 20m/s to 45m/s.

4.3 Estimation of the dissipation rate ϵ

The dissipation rate has been estimated from the inertial range dynamics of the turbulence. More precisely, we use the well-known scalings for the second order Eulerian longitudinal structure function ($S_2^{\parallel}(\rho)$) and the third order Eulerian longitudinal structure function ($S_3^{\parallel}(\rho)$). Recall that the Eulerian longitudinal structure function of order n is defined as the nth moment of the longitudinal velocity increment $\delta u(\rho) = u(x+\rho) - u(x)$: $S_n^{\parallel}(\rho) = \langle \delta u^n \rangle$. In the Kolmogorov 1941 framework, the scaling $S_n^{\parallel}(\rho) \propto (\epsilon\rho)^{n/3}$ is expected for inertial range spatial increments ρ, although intermittency corrections (which will not be discussed here) are known to apply for high order (typically $n > 4$)

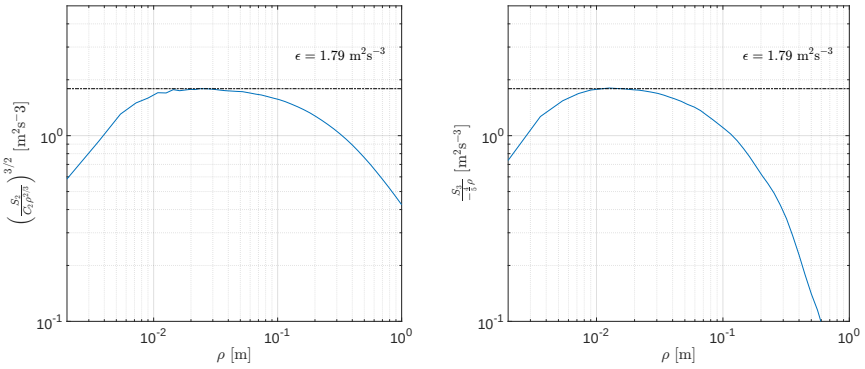

(a) (b)

Fig. 10 (a) Second order longitudinal structure function, compensated by the Kolmogorov scaling, with $C_2 \approx 2.1$, measured at $X/M \approx 37$ and a mean wind speed of $45m/s$. The plateau gives an estimate of the energy dissipation rate ϵ. (b) Compensated third order longitudinal structure function.

structure functions. Here, we estimate epsilon, based on the well-known scaling for $S_2^{\parallel}$ and $S_3^{\parallel}$ at large Reynolds numbers :

$$S_2^{\parallel}(\rho) = C_2 \left(\epsilon\rho\right)^{2/3}, \tag{5}$$

$$S_3^{\parallel}(\rho) = C_3 \left(\epsilon\rho\right), \tag{6}$$

$$\tag{7}$$

where C_2 is empirically known to be approximately 2.1 [12] and C_3 can be derived analytically (under certain assumptions of homogeneity, stationarity and in the limit of large Reynolds numbers) from the Navier-Stokes equations and is equal to -4/5 [6]. Figures 10a and b show the second and third order compensated longitudinal structure functions for the measurements at $X/M \approx 37$ and a mean wind speed of $45m/s$. In both plots, the plateau is expected to give an estimate of the energy dissipation rate ϵ. We find that both estimates are indeed identical. The energy dissipation rate is found to increase from $0.20to2.5m^2/s^3$ when the mean wind-speed increases from $20m/s$ to $45m/s$.

4.4 Estimation of the dissipation scales and the Taylor-scale Reynolds number

Once the dissipation rate ϵ is known, the dissipation scale η and the dissipation time τ_η are estimated from the classical relations :

$$\eta = \left(\frac{\nu^3}{\epsilon}\right)^{1/4}, \tag{8}$$

$$\tau_\eta = \left(\frac{\nu}{\epsilon}\right)^{1/2}. \tag{9}$$

Similarly, the Reynolds number R_λ based on the Taylor micro-scale can be estimated as

$$R_\lambda = \frac{\sigma_u \lambda}{\nu}, \tag{10}$$

with $\lambda = \sigma_u \sqrt{15\nu/\epsilon}$ the Taylor micro-scale of the flow.

In this experiment, when the wind speed increases from $20m/s$ to $45m/s$, the dissipation scale η decreases from about 370 μm to about 200 μm, the dissipation time scale decreases from about 9ms to about $2.5ms$ and the Reynolds number based on Taylor micro-scale increases from about 300 to about 500.

4.5 Summary of turbulent properties

The table 1 summarizes the main characteristics of the turbulence produced at $X/M \approx 37$ (*i.e.* the farthest position to the grid tested). Signals from experiments closer to the grid are still been processed to address the decay properties of turbulence downstream of the grid.

U [m/s]	σ_u [m/s]	L [m]	T_E [s]	ϵ [m^2s^{-3}]	η [μm]	τ_η [ms]	λ [mm]	R_λ
20	0.36	0.15	0.42	0.20	365	8.9	12.3	295
25	0.41	0.15	0.37	0.30	330	7.2	11.5	320
35	0.58	0.16	0.27	0.81	260	4.6	9.8	380
45	0.79	0.18	0.21	2.4	195	2.4	8.4	490

Table 1 Summary of main properties of the turbulence produced at $X/M \approx 37$ (the farthest position from the grid tested in this experiment)

5 Conclusion

In this article, we present the planning and setup of a unique grid turbulence experiment carried out in the S1MA wind-tunnel from ONERA in Modane, in the context of the ESWIRP European project, as well as the first elements of characterization of the turbulence produced, summarized in table 1. This is the largest grid-generated turbulence experiment ever performed. The motivation for such a large scale experiment was not to reach the highest possible Reynolds numbers (dedicated facilities, such as the Variable Density Turbulent Tunnel at the Max Planck Institute of Göttingen and the GReC jet in CERN are specifically designed for that) but to resolve the full range of scales in homogeneous isotropic turbulence, including the smallest dissipative scales. This goal has been reached for most of the hot-wire anemometry measurements collected, as shown by the Eulerian spectra in figure 4c. Additionally, the estimation of dissipative scales in table 1 shows that the smallest value of η is of the order of 200 μm. Although this is marginally smaller than our classical hot-wires (which had a sensitive length of the order of 400 μm), one

should keep in mind that the actual transition to dissipation dynamics occur at scales typically 15 times larger than η [4], *i.e.* or the order of 3 mm, which are indeed fully resolved by most of our probes. Finally, the amount of data acquired during this campaign ensures very accurate statistical convergence. Finally, the present measurements constitute a highly-resolved database of canonical grid-generated turbulence, which we hope will serve the community seeking to probe new ideas in order to unveil the open questions presented by turbulence. If interested in this data, please contact Mickaël Bourgoin: mickael.bourgoin@ens-lyon.fr.

5.1 Acknowledgments

We acknowledge the European Union for its support via the ESWIRP project (FP7/2007-2013 under grant agreement No. 227816) for the access to the S1MA wind-tunnel from ONERA and the EuHIT project (grant agreement No. 312778) for probes development. We thank the CNRS, the Ecole Normale Supérieure de Lyon (France), the CORIA (Rouen, France) the Institut Néel and the LEGI (Grenoble, France) for their financial support. We are extremely grateful to the ONERA, and in particular to Jean-François Piat, Bernard Genoulaz and Emmanuel Durieux, for their help and precious technical support without whom the realization of this experiment would have never been possible. We are also grateful to Pierre Jaricot, from Certec®, for his advice and expertise for the design and manufacturing of the inflatable grid.

This manuscript is dedicated to the memory Carine and Joël. They will never be forgotten.

References

1. A Arneodo, C Baudet, F Belin, R Benzi, B Castaing, B Chabaud, R Chavarria, S Ciliberto, R Camussi, F Chillà, B Dubrulle, Y Gagne, B Hebral, J Herweijer, M Marchand, J Maurer, J. F Muzy, A Naert, A Noullez, J Peinke, F Roux, P Tabeling, W. van de Water, and H Willaime. Structure functions in turbulence, in various flow configurations, at Reynolds number between 30 and 5000, using extended self-similarity. *Europhysics Letters (EPL)*, 34(6):411–416, may 1996.
2. A Arneodo, R Benzi, J Berg, L Biferale, E Bodenschatz, A Busse, E Calzavarini, B Castaing, M Cencini, L Chevillard, R T Fisher, R Grauer, H Homann, D Lamb, A S Lanotte, E Leveque, B Luethi, J Mann, N Mordant, W C. Mueller, S Ott, N T Ouellette, J F. Pinton, S B Pope, S G Roux, F Toschi, H Xu, and P K Yeung. Universal intermittent properties of particle trajectories in highly turbulent flows. *Physical Review Letters*, 100(25):254504, 2008.
3. Sean C. C. Bailey, GARY J. Kunkel, Marcus Hultmark, Margit Vallikivi, Jeffrey P. Hill, Karl A. Meyer, Candice Tsay, Craig B. Arnold, and Alexander J. Smits. Turbulence measurements using a nanoscale thermal anemometry probe. *Journal of Fluid Mechanics*, 663:160–179, sep 2010.
4. Laurent Chevillard, Bernard Castaing, Alain Arneodo, Emmanuel Lévêque, Jean François Pinton, and Stéphane G. Roux. A phenomenological theory of Eulerian and Lagrangian velocity fluctuations in turbulent flows. *Comptes Rendus Physique*, 13(9-10):899–928, 2012.

5. G. Comte-Bellot and S. Corrsin. Simple Eulerian time correlation of full- and narrow-band velocity signals in grid-generated 'isotropic' turbulence. *Journal of Fluid Mechanics*, 48:273–337, 1971.
6. U Frisch. *Turbulence: The Legacy of A. N. Kolmogorov*. Cambridge University Press, Cambridge, England, 1995.
7. A. N. Kolmogorov. Dissipation of energy in the locally isotropic turbulence. *Dokl. Akad. Nauk SSSR*, 32:16–18, 1941.
8. A N Kolmogorov. Refining the Notions of the Local Structure of Turbulence in an Incompressible Viscous Fluid at High Reynolds Numbers. In *Mecanique de la turbulence*, pages 447–458. CNRS, Paris, 1962.
9. Stephen B Pope. *Turbulent flows*. Cambridge University Press, Cambridge, England, 2000.
10. Jaroslaw Puczylowski, Michael Hölling, and Joachim Peinke. Measurements with a 2D Laser-Cantilever-Anemometer compared to an x-wire probe. *Proc. Appl. Math. Mech.*, 2(0):1–2, 2009.
11. J. P. Richter. Plate 20 and Note 389. In *In the notebooks of Leonardo da Vinci*. Dover, New York, 1970.
12. Katepalli R Sreenivasan. On the universality of the Kolmogorov constant. *Physics of Fluids*, 7(3):2778–2784, 1995.
13. A. Vincent and M. Meneguzzi. The spatial structure and statistical properties of homogeneous turbulence. *Journal of Fluid Mechanics*, 225(1):1–20, 1991.